Department of Energy
Grant No. DE-FG03-00-ER45808
FINAL REPORT

Submitted by
Joseph H. Simmons and Tracie J. Bukowski
University of Arizona
Tucson, AZ 85721

Quantum Confinement, Carrier Dynamics and Interfacial Processes in Nanostructural Direct/Indirect-Gap Semiconductor-Glass

Abstract

This grant was a continuation of research conducted at the University of Florida under Grant No. DE-FG05-91ER45462 in which we investigated the energy bandgap shifts produced in semiconductor quantum dots of sizes between 1.5 and 40 nm. The investigated semiconductors consisted of a series of Column 2-6 compounds (CdS, CdSe, CdTe) and pure Column IV elements (Si and Ge). It is well-known of course that the 2-6 semiconductors possess a direct-gap electronic structure, while the Column IV elements possess an indirect-gap structure. The investigation showed a major difference in quantum confinement behavior between the two sets of semiconductors. This difference is essentially associated with the change in bandgap energy resulting from size confinement. In the direct-gap semiconductors, the change in energy (blue shift) saturates when the crystals approach 2-3 nm in diameter. This limits the observed shift in energy to less than 1 eV above the bulk value. In the indirect-gap semiconductors, the energy shift does not show any sign of saturation and in fact, we produced Si and Ge nanocrystals with absorption edges in the UV. The reason for this difference has not been determined and will require additional experimental and theoretical studies. In our work, we suggest, but do not prove that mixing of conduction band side valleys with the central valley under conditions of size confinement may be responsible for the saturation in the blue-shift of direct-gap semiconductors.

The discovery of large bandgap energy shifts with crystal size prompted us to suggest that these materials may be used to form photovoltaic cells with multi-gap layers for high efficiency in a U.S. Patent issued in 1998. However, this possibility depends strongly on the ability to collect photoexcited carriers from energy-confined crystals. The research conducted at the University of Arizona under the subject grant had a major goal of testing an indirect gap semiconductor in size-confined structures to determine if photocarriers could be collected. Thus, we tested a variety of semiconductor-glass nano-composite structures for photoconductivity. Tests were conducted in collaboration with the Laser Physics Division at Sandia National Laboratories.

Nano-composite samples were formed consisting of Ge nanocrystals embedded in an indium-tin-oxide matrix. Photoconductivity measurements were conducted with exposure of the films to

sub-bandgap and super-bandgap light. The results showed a clear photoconductivity effect arising from exposure to super-bandgap light only. These results suggest that the high-efficiency photovoltaic cell structure proposed in DOE sponsored U.S. Patent 5,720,827 is viable. The results of fabrication studies, structural characterization studies and photovoltaic measurements are presented in the report.

This report is taken from a PhD dissertation of Tracie J. Bukowski submitted to the University of Florida in May 2002. "The optical and photoconductive response in germanium quantum dots and indium tin oxide composite thin film structures," Dr. Bukowski conducted her PhD study under this grant at the University of Arizona and under Grant No DE-FG05-91ER45462 at the University of Florida, as well as during a two-year fellowship at Sandia National Laboratories.

Introduction

Quantum dots offer can be fabricated in different sizes and can exhibit a range in band gap energies that increase (blue shift) with decreasing crystal size. Past studies with direct gap semiconductors (CdS and CdTe) have shown a saturation in the blue shift at small crystal sizes [1]. Recent studies of Ge quantum dots show no saturation. This is shown in the broad range of absorption edges exhibited by Ge nanocrystals varying in size between 0.4 nm and 15 nm. Note that the very small films are transparent in the visible and begin to absorb near UV wavelengths.

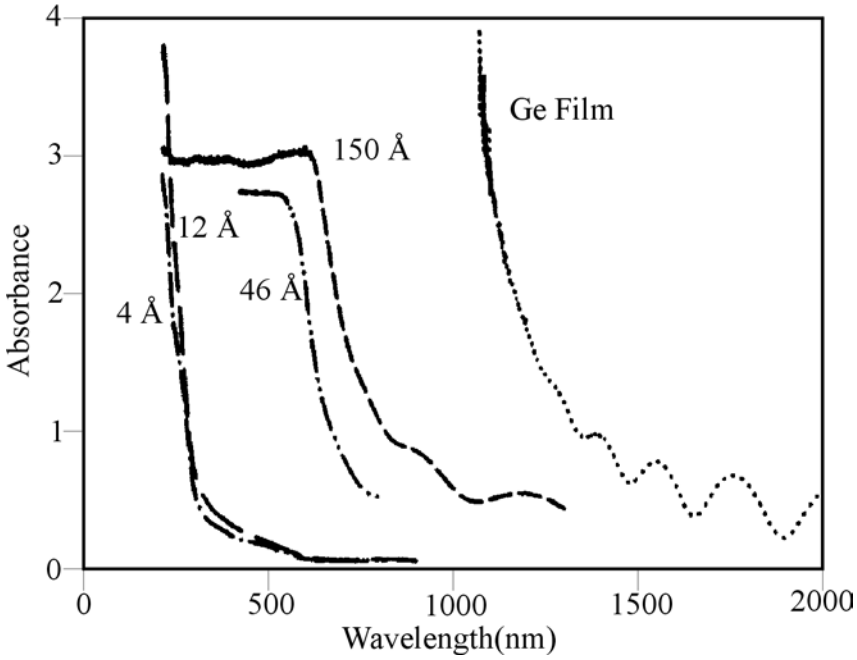

Figure 1 Absorbance versus wavelength for a Ge film and for various Ge quantum dots 150 Å, 46 Å, 12 Å, and 4 Å in diameter [from Ref. Xxx]

The curve shown in the figure is from Bukowski et al. [1] and reports data on germanium quantum dots in a SiO_2 matrix. This absorbance data illustrate the dramatic shift in band gap that is possible with varying the dot size (see Fig. 1). As can be seen, a blue-shift in energy results as one goes from a thin film of Ge to quantum dots of Ge 4 Å in diameter. In fact the shift in band gap energy spans several eVs. The data prove that not only does quantum confinement of the Ge quantum dots produce a dramatic blue-shift in band gap energy, but that the size of the dots produced can be tailored to vary E_g over a wide range of desirable values.

However, if the special qualities of quantum dots are to be utilized in a photoconductive or photovoltaic device, such as a solar cell [2], photoexcited carriers must diffuse into the matrix material. This is only possible if the matrix material is not only transparent, but also electrically conducting. This becomes the basis for the current research – "What happens when the insulating SiO_2 matrix is replaced with a transparent conducting oxide matrix?" The implications of such a question are important and numerous. The goal of this research was to show experimentally that the presence of semiconductor quantum dots inside the transparent conducting matrix produces an enhanced electrical photoresponse.

Photoconductivity is a phenomenon where extra carriers are generated within a semiconductor or insulator when it is illuminated by photons of the appropriate energy [3]. The presence of the photogenerated carriers results in a lowering of the resistance of the material, i.e. the electrical conductivity is enhanced. This effect, however, is only measurable under the influence of an electric field, whether it is inherent in the material or externally applied. Hence, photoconductivity is a two-step process whereby excess carriers are first generated optically, and then transported across the material by an electric field. The energy, or wavelength (λ_p), of light necessary for creating the photoexcited carriers is determined by the band gap, E_g, of the material. So, for all wavelengths of light equal to or less than λ_p, the energy is absorbed to produce electron–hole pairs.

When a semiconductor thin film is illuminated, generating an electron-hole pair, both the electron and the hole can contribute to the resulting conductivity. In all of the treatments of the issue of conductivity there are two important terms that help define the conductive behavior of a material. These terms are the density of free carriers, n, and the mobility of the carriers, μ. Of the two, the density of carriers often has a more dramatic effect on conductivity, as it is more strongly a function of energy. When both the electron and hole contributions to the overall conductivity are considered, the final expression is

$$\sigma = q(n\mu_n + p\mu_p) \qquad (2\text{-}6)$$

where q is the electronic charge of the carrier, n and p are the number of electrons and holes, and μ_n and μ_p are the corresponding electron and hole mobilities, respectively. Clearly, by increasing the number of carriers, both electrons and holes, and their corresponding mobilities, the conductivity of the material can be increased.

However, the process of excitation and enhanced conductivity can be complicated by various mechanisms that interfere with the successful transport of any excited carriers. When photoexcitation produces a free hole and free electron, both carriers will contribute to the increased conductivity as long as they are unhindered and pass out of the material at the appropriate contact end, while being replaced at the other contact end to maintain charge neutrality. For a material with defects, the carriers can be captured by local imperfections, or the electron and hole can simply recombine. Often, recombination occurs between a trapped carrier and a free carrier of opposite type, or also by two closely trapped carriers. The ultimate effect is that the carrier density is decreased, which reduces the enhanced photoconductive response.

Such carrier trapping sites can have a pronounced effect on the dynamics of carrier transport, specifically in photoexcited carrier decay time. Imagine that a photoconducting material is illuminated, exciting carriers at a rate of g_o carriers per second-cm^3. The conductivity increases and reaches a steady state when the excitation source is turned off. Without the excitation source providing energy for continued production of carriers, those in excited states will begin to decay to their ground states. The rate at which this occurs can offer an insight into the number of trapping sites in a material. Consider the case where the number of electrons in traps, n_t, is much smaller than the density of free electrons, n. This is known as trap saturation and is common at high excitation levels or high temperature. In such a situation, the current will decay exponentially, with a decay time equal to the electron lifetime τ_o. Knowing τ_o makes it possible to calculate the microscopic mobility of the majority carriers, μ_o [3].

$$\Delta\sigma = qg_o\tau_o\mu_o \quad (2\text{-}7)$$

However, if instead the number of free electrons is much smaller than the number of trapping sites, then the decay can be significantly longer due to slow release of carriers from their trap sites.

While the relative intensity of the light source can affect the decay rates, the type of traps present also has a pronounced effect in the decay behavior. In n-type silicon (n-Si), studies have been done to evaluate the decay time in photoconductivity experiments [4]. Figure 2(a) shows a typical rise and decay curve for n-Si, illustrating the effect that trapping sites have on the resulting measured behavior [4]. In this case, shallow traps, as indicated by the short decay times, dominate the decay behavior. The light source is turned on at point A, creating electrons and holes which increase the conductivity to point B where they reach equilibrium. Between B and C, hole trapping occurs, causing the overall conductivity rate to decrease somewhat. The light is then turned off at point C and a decay is observed corresponding to the recombination of excess electrons and holes between C and D. Finally, the shallow traps are emptied resulting in the slower decay rate seen between points D and E.

A similar trend is seen for n-Si containing deep level traps. Figure 2(b) presents the photoconductivity curve, illustrating the typical long-time decay behavior associated with deep hole traps. When the light source is removed, the expected drop in conductivity is seen between D and E. This initial fast decay corresponds to recombination and the emptying of shallow traps. The deep traps are represented in the region from E to F and can take considerably longer to decay. Such a curve can provide quantitative information, allowing the calculation of the density of deep traps from the difference in conductivity between D and F [4].

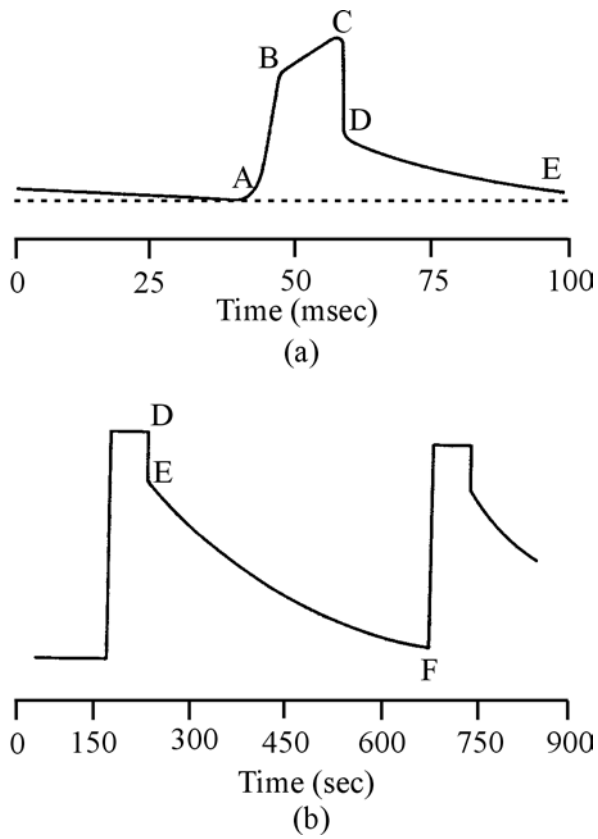

Figure 2 Rise and decay curves of photoconductivity for n-type silicon with (a) shallow traps and (b) deep traps.

Clearly, the rate at which the measured photoconductive response of a material decays when the light is turned off is dependent on the type of process taking place. The fastest decay rate process, alluded to in the above example, is the direct recombination of free electrons and holes. The next fastest decay process is the emptying of shallow traps. The slowest decay rate processes are due to the emptying of deep traps and the retrapping of carriers.

The major problem to the production of photoconductivity in semiconductor-glass composites arises from the presence of a potential energy barrier to carrier transport due to the presence of confinement. This barrier height can be different for the electrons and holes of the excited exciton, and, thus, each can contribute in different ways. It is important in the material selection process that the band diagrams be considered for insight into the potential electronic behavior of the confined carriers. Too high a potential barrier can make transporting the carriers to the electrodes difficult. Too low a barrier and confinement will not be present.

While the dynamics involved in photoconductivity can be very complex, by measuring the conductivity in both dark and illuminated conditions any resulting gain can be measurable. It is expected that the presence of the germanium dots will effectively increase the carrier density available for transport, resulting in an increased photoresponse. Furthermore, the rate at which the excited carriers decay back to their ground state can offer an interesting look into the density of trapping sites.

Thin Film Fabrication

Materials Selection

Clearly, the matrix material needs to be conductive and transparent over the wavelength spanning the range of observed bandgaps for the quantum-confined semicondutors. A class of doped and non-stoichiometric oxide materials has been used as transparent conducting oxides for many different purposes such as transparent electrodes. Of these, the most popular and that with the largest window is indium tin oxide (ITO) [5, 6]. Work done by Chopra et al. has produced a review of transparent conductors, including ITO [7]. Figure 3 shows graphically how various oxides rate for transmission and resistance properties. ITO is compared with other transparent conducting oxides such as zinc oxide (ZO), tin oxide (TO) and antimony tin oxide (ATO). Clearly, ITO films possess one of the highest percent transmission, %T, and are among the lowest in measured sheet resistance, R_s. ITO has been one of the most widely used and successful transparent conductors, and is well known for its high transparency in the visible region of the spectrum (>80%), strong reflectance in the infrared region and high radiation resistance [8, 9]. In order to understand where ITO obtains its superior properties, we must first discuss the mechanisms behind its conductivity and optical transparency.

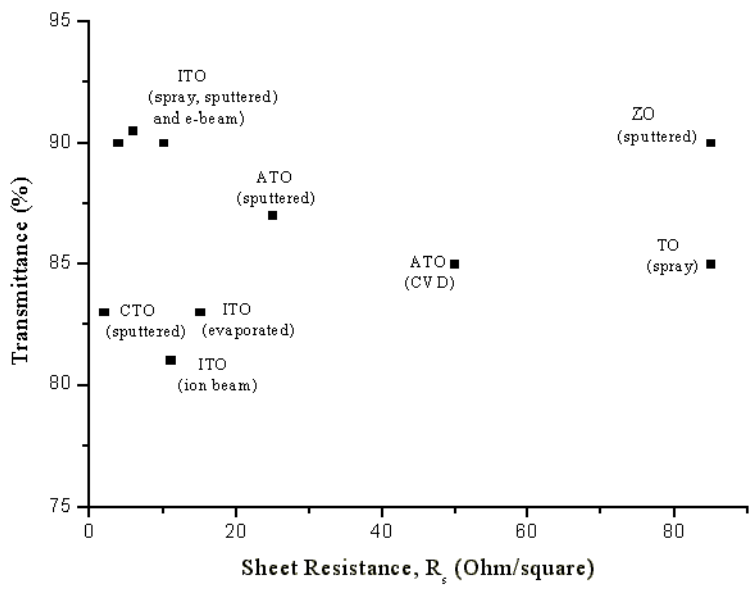

Figure 3 Transmittance and sheet resistance for various transparent conducting oxides; Note: fabrication method identified in parentheses.

In the undoped state, indium oxide (IO) films are generally polycrystalline with a cubic bixbyte structure, a lattice constant, a, of 10.118 Å, and a typical grain size of about 100 Å. IO is considered a semiconductor with a direct band gap of 3.5 eV and an indirect gap of 2.5 eV. It is an n-type conductor, meaning that the primary carriers are electrons produced from oxygen vacancies in the film. Doping with tin (Sn), to create indium tin oxide (ITO), enhances its conductivity. ITO films have the same structure as IO but have

a small change in the lattice constant, 10.118 Å<a<10.31 Å, with grain sizes typically between 400 and 600 Å, and a direct band gap generally greater than 3.5 eV.

Typical tin doped In_2O_3 films have a measured resistivity in the range of 7x10-5 to 5x10-4 Ω-cm. The effect of doping In_2O_3 with Sn is an increase in the density of free electrons. Figure 4 illustrates the change in the density of free electrons with the %Sn doping concentration in In_2O_3. Initially, the free electron density, and hence the conductivity, increases over the first few percent Sn doping concentration, following a straight line indicated by curve (a). If extrapolated to 100% Sn doping, curve (a) would reach a value consistent with the number of In atoms in In_2O_3, implying that Sn substitutionally takes the position of the In in the In_2O_3 lattice. Because of the electron valencies of the two atoms, In being +3 and Sn being +4, the act of substituting Sn on an In site produces an extra electron, thereby enhancing the free electron density. However, as Figure 4 clearly shows, a departure from this proposed linear behavior, and a marked decrease in the carrier density at doping levels above a few percent Sn [10]. The presence of a maximum in the free carrier density as a function of Sn doping is due to interactions between the Sn atoms that occur as they begin to come in close contact [10]. As a result, there is an optimum doping level in Sn:In_2O_3 that generates the lowest film resistivity, which occurs around 10% Sn.

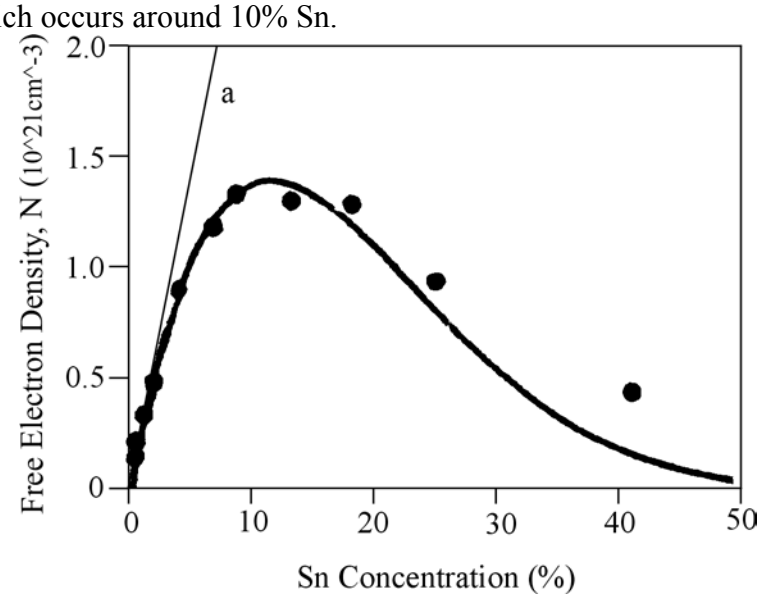

Figure 4 Free electron density of states as a function of % Sn doping in In_2O_3.

The change in the free electron density in ITO films, due to the incorporation of tin, also has a pronounced effect on its optical behavior. Figure 5 shows typical absorbance, A, transmittance, T, and reflectance, R, curves for an ITO film [11]. Absorbance is the fraction of light absorbed by the material relative to the incident light. Transmittance is that fraction of light that passes through the material, and reflectance is that which is reflected at the surface. Note that the oscillations seen at the short wavelengths are Fabry-Perot interference oscillations resulting from the measurement of a thin film. ITO is characterized by a high optical transparency in the visible and near-IR regions, but is limited due to reflection losses at the surface (1-2%) and absorption in the film (1-2%) due to free carrier absorption. This effect of free carrier absorption becomes

pronounced in the near-IR as evidenced by the sharp onset of reflection. This behavior can be modeled using classical Drude theory, which describes the plasma oscillation of the free electrons through the equation,

$$\lambda_p = 2\pi c\left(\frac{4\pi N e^2}{\varepsilon_M m_c}\right)^{-1/2} \qquad (3\text{-}1)$$

where ε_M is the dielectric constant of the material, m_c is the effective mass for electrons in the conduction band, and N is the free electron density. The plasma frequency, λ_p, is by definition the wavelength at which the real part of the complex dielectric constant, ε_r, is equal to zero. The observed absorption peak that occurs with the rise in reflection is due to plasma resonance. For $\lambda > \lambda_p$, ε_r is negative, and as a result, the plasma is reflective, coinciding with the R onset in the spectrum. It is important to note that the free electron density affects where the wavelength of the plasma resonance occurs. As the free electron density increases, the plasma wavelength shifts towards shorter wavelengths, i.e. higher energies. Hence, the free carrier density in ITO can greatly alter the transparency region in these films.

In addition to affecting the near-IR reflection, the density of free carriers also influences the UV absorption edge in ITO. Similar to the plasma oscillation, an increase in the free electron density results in a blue-shift in the intrinsic absorption edge. This effect is known as the Moss-Burstein shift and is due to a filling of states in the conduction band. As the number of free electrons is increased, the conduction band begins to fill at the bottom, essentially forcing the bottom of the conduction band to higher energies. Assuming parabolic band edges, this shifting in the band edge energy can be described by

$$\Delta E_{M-B} = \frac{h^2}{8m_{vc}^*}\left(\frac{3N}{\pi}\right)^{2/3} \qquad (3\text{-}2)$$

where N is the free electron density and m_{vc}^* is the conduction band effective mass, which also considers valence band curvature effects. In the discussion of the absorbance data in a later chapter, it will be important to consider all potential reasons for a shift in the band edge of the quantum dot films. This is especially true since a blue-shift in the absorption edge is also an obvious response in a film due to quantum confinement effects.

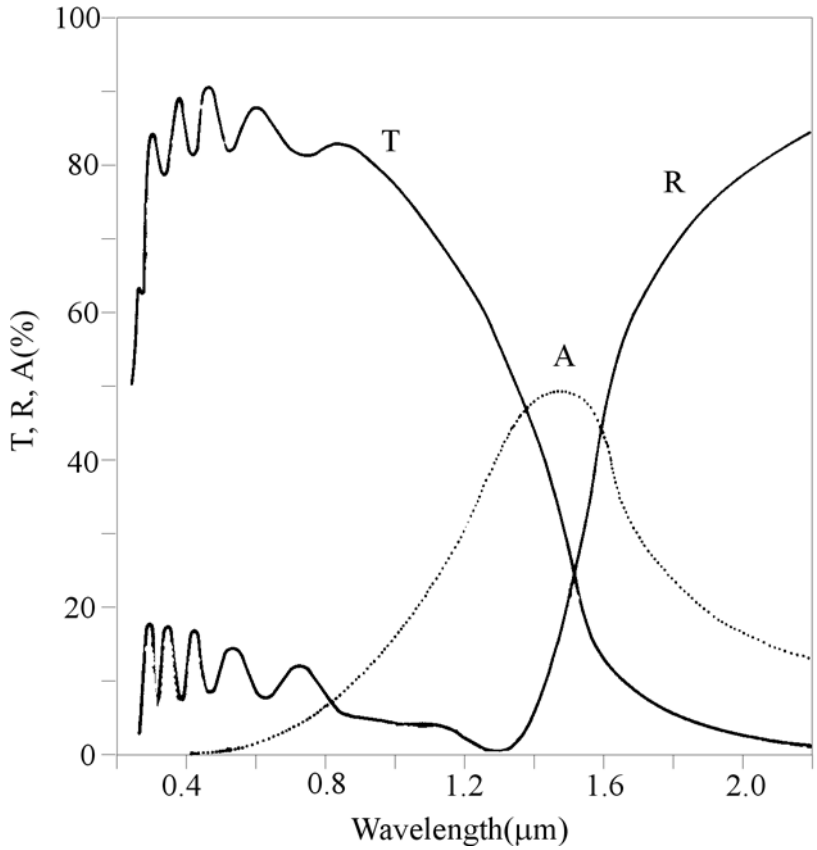

Figure 5 Typical absorbance, A, transmittance, T, and reflectance, R, curves for an ITO film.

Finally, there are certain changes in the resistivity and optical behavior of ITO as a result of thermal annealing. Because applying a heat treatment to the nanocomposite films is an important step in developing the quantum dot, as discussed in section 3.3, it is necessary to understand the influence that temperature can have on the properties of ITO [12-15]. The two most prominent reactions that occur in ITO films during thermal anneals are grain growth and oxygen diffusion into the films, both of which can have pronounced effects on the resulting electrical and optical properties. ITO, in its as-deposited state, has a pale yellow appearance. At temperatures around 100-200°C, the films become clear, losing their color. This happens because of a rapid grain growth process that occurs at these temperatures, removing any absorbing defects. As this process takes place, the conductivity is also greatly increased as the rapid grain growth spurs an increase in the oxygen vacancy concentration [12]. Because oxygen vacancies are so vital to the film's conductivity, it is important to note that the atmospheric partial pressure of oxygen inside the furnace can profoundly affect the resistivity. Often, an inert gas or a reducing gas environment is passed through the furnace to displace any atmospheric oxygen that might be present.

Assuming that the oxygen partial pressure during heat treatment is sufficiently low, then the effects of grain growth dominate the changes that happen in resistivity and absorption. Initially, the decrease in resistivity is rapid as many new carriers are created

due to an increase in oxygen vacancies. But above around 200°C, the resistivity tends to flatten out. At this point grain growth slows down, and any further decrease in resistance is due to mobility contributions as a result of any grain size increases. In general, the point to make is that, in the proper atmosphere, an increase in temperature results in an increase in carrier density, carrier mobility, and, hence, an increase in conductivity and transparency.

Given all of the data published on ITO films and the effects that various parameters, such as deposition method, dopant concentrations, and temperature, have on the resulting electrical and optical properties, it is important to understand these effects [7, 10-25]. In the case of this research, ITO was chosen because of its superior conductivity and high transparency region. Two major conditions dictated the choice of semiconductor nanocluster: (1) the material must be easily made into nanocrystals and should possess large energy shifts with crystal size; (2) it is necessary that the quantum dot material does not interact strongly with the matrix material, for example, a material that forms an oxide coating around the dot would prevent carrier transport.

Considering all of the important criteria, germanium was chosen for the quantum dot material. Germanium is a popular material for synthesizing quantum dot structures using many different deposition techniques, indicating that ease of fabrication is achievable [26-29]. Based on electronic structure and the band gap energy of the bulk material, both Si and Ge make interesting candidates. Both exhibit a large shift in energy, ΔE, with size as was shown earlier. However, their oxidation energy is very different. The formation of an oxide at the interface of the quantum dot and the ITO matrix material would greatly affect the electrical properties of the films since intrinsic oxides are known dielectrics. In such a situation, even if carriers were created within the quantum dot, they would be prohibited from being transported across the junction and, hence, no enhanced photoconductivity would be measured. Table 1 compares the oxygen dissociation energies for various oxides [30]. When comparing germanium dioxide, GeO_2, and silicon dioxide, SiO_2, with the ITO components (indium oxide, In_2O_3 and tin oxide, SnO_2), it is clear that Si will take oxygen from both, while Ge is less likely to do so. In_2O_3 is a more stable oxide than GeO_2, and SnO_2 is only slightly less stable than GeO_2. This table indicates that Ge is less likely to oxidize in ITO than Si. However, some care is necessary since the GeO_2 dissociation energy is greater than that for SnO_2.

Table 1 Dissociation energy per oxygen atom for various molecules.

Molecule	Dissociation Energy (kcal/mol)
SeO_2	27.5
TeO_2	38.8
Bi_2O_3	46.0
CdO	60.9
SnO_2	69.4
GeO_2	96.3
TiO_2	109.0
In_2O_3	111.3

CeO_2	122.5
B_2O_3	150.9
SiO_2	153.9
Al_2O_3	195.9

Several of the important materials properties associated with bulk germanium are listed in Table 2 [31, 32].

Table 2 Basic materials properties of Germanium.

Lattice Constant (Å)	Density (g/cm^3)	Dielectric Constant	Energy Gap (eV)	Melting Point (°C)	Refractive Index	Intrinsic Resistivity (Ωcm)
5.66	5.32	16.0	0.67	937	4.0	47

Sapphire was chosen for the substrate. Sapphire is a synthetic crystal form of aluminum oxide, Al_2O_3, with a hexagonal crystal structure. The transmission of sapphire is excellent, limited primarily by surface reflections. In the wavelength regions extending from visible through infrared, sapphire transmits well over 80% of the incident photons. In addition, sapphire is chemically inert, and is extremely hard, ranking 9 on the Moh's hardness scale [33]. Finally, with respect to its temperature dependent properties, sapphire has a coefficient of thermal expansion of 7.7x10-6/°C (compared to 7.2x10-6/°C of ITO) and a softening point of 1800°C [33]. Table 3 provides a list of some of the fundamental materials properties of sapphire.

Table 3 Basic materials properties of sapphire.

Density (g/cm^3)	Softening Point (°C)	Refractive Index	Moh Hardness	Coefficient of Linear Expansion (/°C)
3.98	1800	1.8	9	$7.7x10^{-6}$

RF Magnetron Sputtering

Many techniques have been used in creating Ge quantum dots, including ion implantation, inorganic solution phase synthesis, dc magnetron co-sputtering and rf co-sputtering [26-28, 34, 35]. It was discovered within our laboratories that a dual gun, rf magnetron sequential sputtering technique [35] was very successful in creating Ge quantum dots within a SiO_2 matrix [1]. This served as a basic model for the fabrication of Ge within ITO. The method consists of alternately exposing a substrate to two separate rf magnetron sputtering guns. Each gun is fitted with a different target, one containing the ITO glass and one containing the Ge semiconductor material. By varying the amount of time that the substrate is held over each target and the deposition rate at each gun, the

relative volume fraction of semiconductor present in the sample can be varied. The result is a multilayer, thin film made up of repeating layers of Ge and ITO.

To create these multilayer films, a substrate is secured onto a sample platter mounted 5 inches above the targets, all enclosed within a stainless steel box chamber. The chamber is evacuated by a turbomolecular pump, which is backed by a roughing pump. The base and operating pressures, $2x10^{-6}$ T and 3 mT respectively, are observed using Penning and thermocouple vacuum gauges [36]. The relative percentage and thickness of each material deposited onto the substrate are completely tailorable by changing the initial computer program input. This automated program would make the necessary calculations based on the user input, and use this to control the rotation of the sample platter by means of a stepper motor. Once the optimum deposition conditions for rf power and chamber vacuum pressure was experimentally determined, a set of investigative samples were prepared.

In order to produce the highest quality film possible, precautions were taken to ensure cleanliness and purity. The substrates were carefully set in a beaker of methanol and placed in an ultra-sonic bath for 30 minutes and then dried with bursts of N_2. During deposition, it is important to note that the substrate was not heated and no gas, other than Ar, was introduced into the chamber. The targets consisted of 2 inch round disks mounted onto their respective guns using silver paste. The ITO target was made up of In_2O_3-SnO_2 (90/10 wt%) of 99.99% purity, and the Ge target was of 99.999% purity.

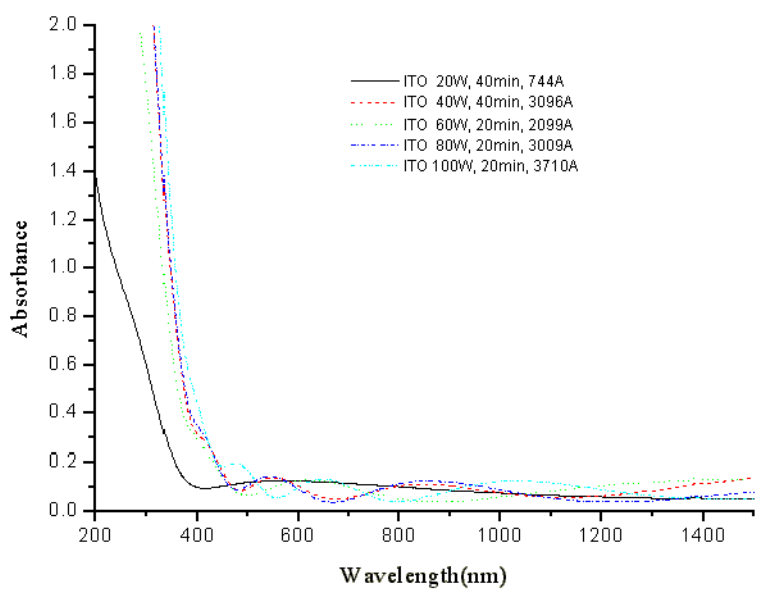

Figure 6 Absorbance versus wavelength for ITO films deposited at different rf powers.

The absorbance and resistivity of the ITO films is quite dependent on the rf power. In fact, the higher the power the higher the resistivity. Figure 6 shows the absorbance of ITO films for different deposition conditions. Figure 7 shows the sheet

resistance vs RF power. The deposition rate was calculated by sputtering an ITO film for a pre-determined amount of time. The resulting film was measured for thickness using a profilometer and averaged over several measurements. With a film thickness and deposition time, a deposition rate was calculated. From this, we calculated deposition rate vs RF power (Fig. 8). As is expected, the rate at which the ITO gun deposits the ITO film onto the substrate increases with applied RF power.

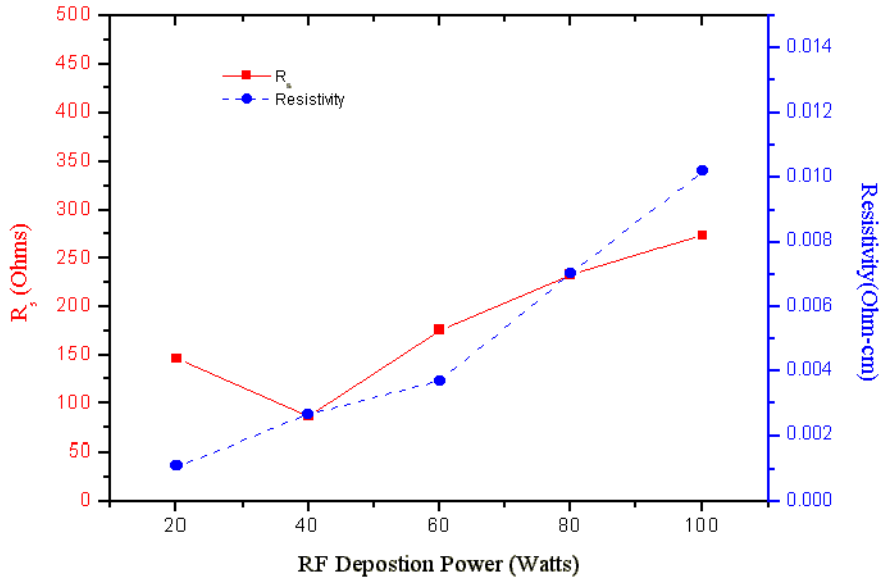

Figure 7 Sheet Resistance and Resistivity of ITO films as a function of RF power.

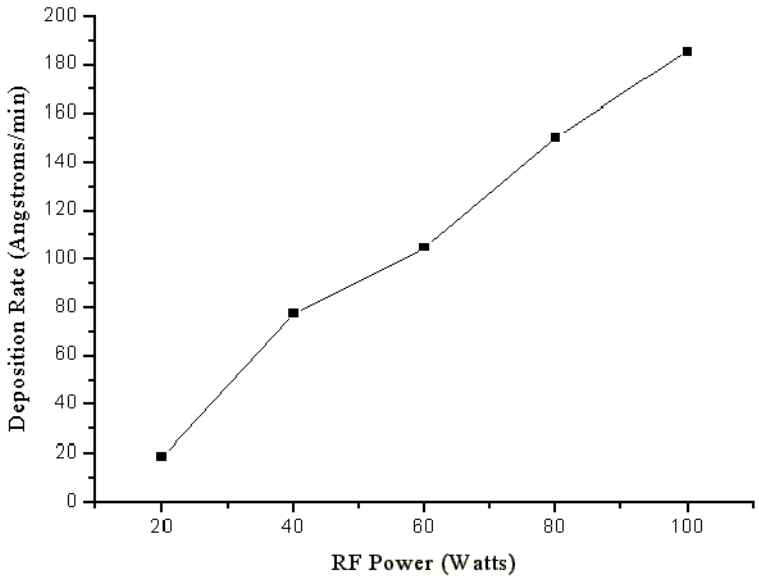

Figure 8 Deposition rate of the ITO gun as a function of RF power.

Quantum Dot Formation

The heat treatments of the multiplayer composite films were performed using a fused silica tube programmable furnace. The films were placed, film side up, in a fused silica boat and positioned in the center of the hot zone of the furnace. The temperature was monitored using two type-K thermocouples; one inside the tube and one just outside, to ensure precise temperature readings. The atmosphere was purged with ultra-high purity Argon (Ar) gas, and was allowed to purge the tube for a minimum of one hour prior to the start of the furnace run. The system was created to minimize the likelihood that outside air was present during anneal; both ends of the tube were capped with silica end-caps that permitted the Ar to flow in one end and out the other through a bubbler. In this way, the ambient air was freed of oxygen, preventing oxidation reactions to occur with the film.

The variables commonly associated with heat treatments are ramp rate, temperature and time. In order to avoid thermal shock from occurring in the film, the ramp should be kept at a reasonable level, typically 10°C/min. Because the material to be grown into crystallites is germanium, the appropriate crystallization temperature must be kept in mind when choosing the anneal temperature. In this case, the crystallization temperature is 630°C, which means that this should be the target temperature. However, in order to understand the dynamics of crystallization and growth of these structures, a series of temperatures were chosen of 600-1000°C. Similarly, several times were used to determine its effect on the resulting film structure, in the range of 6 minutes to 1 hour.

Another important parameter for film fabrication is the relative thickness of each of the germanium and indium tin oxide layers. This is controlled by the volume percent of germanium and its layer thickness. Because the goal is to produce small, isolated clusters of germanium from a layer, it is necessary that the initial layer thickness be sufficiently thin. If the germanium layer is too thick or there is too much of it in the overall film, then quantum dots will not be favored to form during anneals. Also, the volume percent of germanium was kept small in order to promote quantum dot growth and to limit interactions between the dots. For these reasons, the base conditions for creating these quantum dot composite structures were a total germanium content of 5vol% and a layer thickness of 15 Å. These parameters caused the ITO volume percent to be 95% and its thickness to be 280 Å. Previous studies of rf magnetron sputtered Ge, Si and CdTe in SiO_2 has indicated that these fabrication conditions are ideal [37].

Using these initial choices and basic information, a sample matrix was produced. The idea was to be able to make correlations between the variables of temperature, time, Ge vol% and Ge layer thickness in order to determine their impact on the resulting film microstructure and behavior. In the following chapters, insights will be made into how

the processing conditions for the films resulted in specific film morphology, and optical and electrical behaviors.

Microstructure

In order to have a clear understanding of the microstructure or overall physical make-up of the multilayered quantum dot thin films several techniques were used. While it is expected, from previous studies, that from the as-deposited amorphous germanium layers isolated quantum dots will form, it is important to be able to measure their size and determine the structure [37]. From micrographs taken with the transmission electron microscope, TEM, a qualitative evaluation was made of the films as well as a quantitative measurement of the quantum dot size. Further information regarding the compositional constituents present and their relative positions within the film were revealed through automated x-ray spectral imaging (SI) analysis. Details about the crystallinity and structure of the germanium and indium tin oxide were investigated by Raman spectroscopy and x-ray diffraction methods.

All of the films studied consist of germanium (Ge) and indium tin oxide (ITO) alternating layers. The overall Ge content is 5% by volume, corresponding to a nominal germanium layer thickness of 15 Å and ITO layer thickness of 285 Å. The first layer deposited onto the sapphire substrate is always ITO, and the top layer is also always ITO. The range of temperatures used for comparison are the as-deposited state, or heat-treated at 400ºC, 600ºC, 660ºC, or 700ºC, for times of 30-60 minutes as specified. All anneals were done in an argon gas atmosphere. Figures 9 and 10 present the annular dark field STEM images obtained.

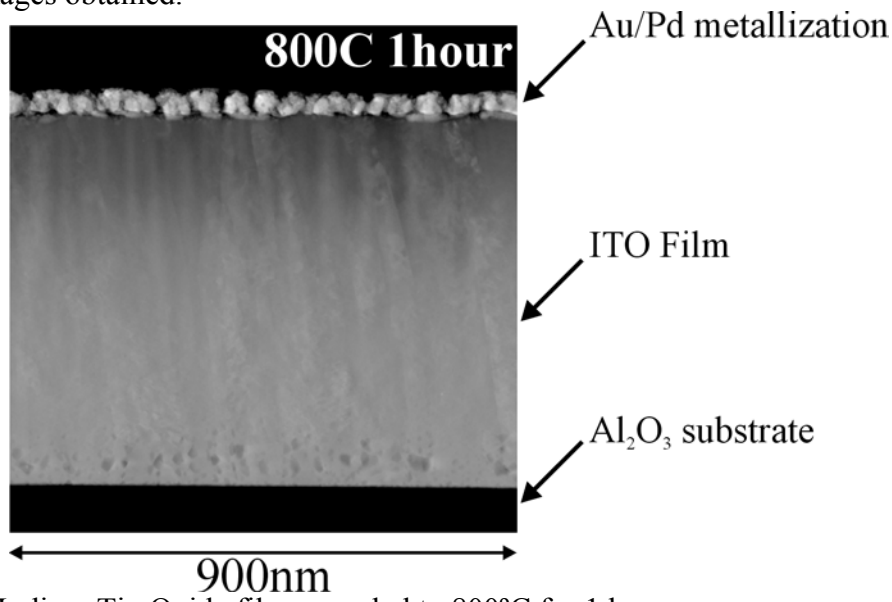

Figure 9 Indium Tin Oxide film annealed to 800ºC for 1 hour.

The pure ITO film was 520 nm thick. The films used in the STM figures were obtained from thinned cross-sections produced by a Focused Ion Beam (FIBS) instrument at Sandia National Laboratories.

Figure 10(a) shows what such a film looks like before any heat treatment has been performed. The structure consists of alternating layers of the Ge and ITO materials. It is a continuous multilayer structure free of voids or quantum dots.

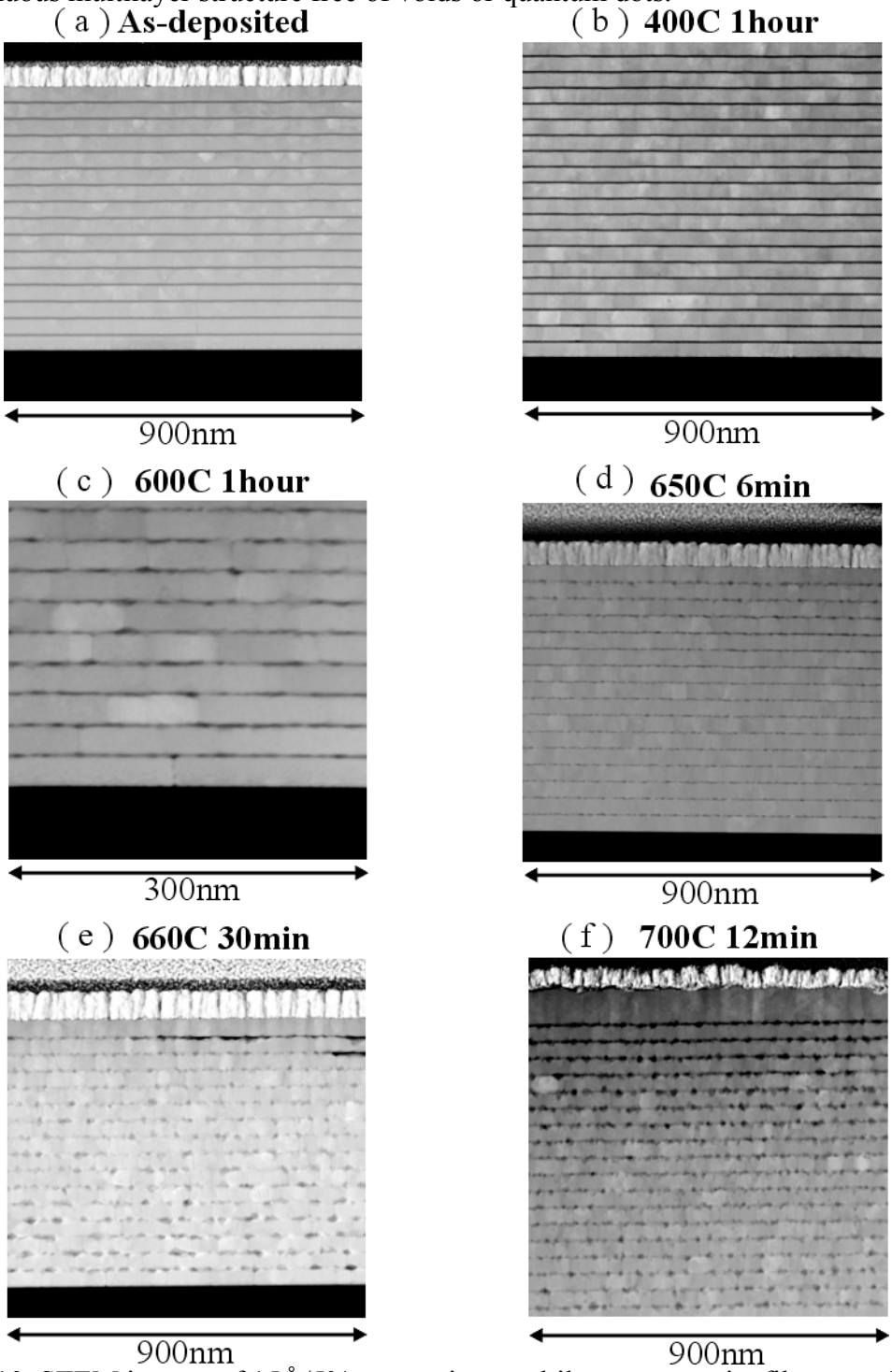

Figure 10 STEM images of 15Å/5% germanium multilayer composite films as a function of temperature (a) as-deposited, (b) 400ºC 1 hour, (c) 600ºC 1 hour, (d) 650ºC 6 minutes, (e) 660ºC 30 minutes, and (f) 700ºC 12 minutes.

The average quantum dot size for the 660°C treated film is 16nm and for the 700°C treated film the average size is 12.6nm. Table 4 presents the calculated average quantum dot sizes for the sample set. For anneal temperatures ranging from 400°C, where no dot formation is apparent, to 700°C, where isolated quantum dots are evident, the range in sizes is only 9 nm – 22nm. The smallest dot size was produced in the film heated to 600ºC for 1 hour, however they were within a somewhat continuous thin Ge layer. The largest quantum dots were found in a film heated to 700ºC for 30 minutes.

Table 4 Average quantum dot sizes for various 15Å/5% Ge multilayer films.

Film Thickness (μm)	Anneal Temperature (ºC)	Anneal Time	Average Quantum Dot Size
1.0	600	1 hour	9 nm (within layer)
0.5	660	30 minutes	11-21 nm
0.5	700	6 minutes	12 nm
1.0	700	12 minutes	12.6-25nm
1.0	700	30 minutes	10-22 nm
1.0	1000	6 minutes	15 nm

X-ray Spectrum Imaging

SI data sets were obtained on the same sample series presented in the STEM images shown in the previous section. Figure 11 presents typical STEM images with the corresponding SI compositional maps, illustrating the evolution of the films with temperature. The point in evaluating the Ge/ITO multilayer films as a function of anneal temperature is to determine what changes are taking place at the different temperatures and to gain insights into the chemical nature of the resulting dot-like structures.

Figure 11 illustrates the chemical signatures detected for a specific region in the 15Å/5% multilayer film heated to 400ºC for one hour . To be clear, the red square shown in the STEM image is the specific area from which the 2-D map was created, typically a 200 nm square section. The software outputs the x-ray spectra detected with a corresponding map. In each case, a separate color-coded map is produced for each chemical signature detected. The pixels colored red indicate the regions where the specific signature is strongest, while blue indicates little or no signal from that signature. At 650ºC for 6 minutes the film has begun to form isolated germanium quantum dots surrounded by indium tin oxide. Finally, the germanium dots grow under anneal conditions of 650-660ºC for 30 minutes and 700ºC for 12 minutes, respectively.

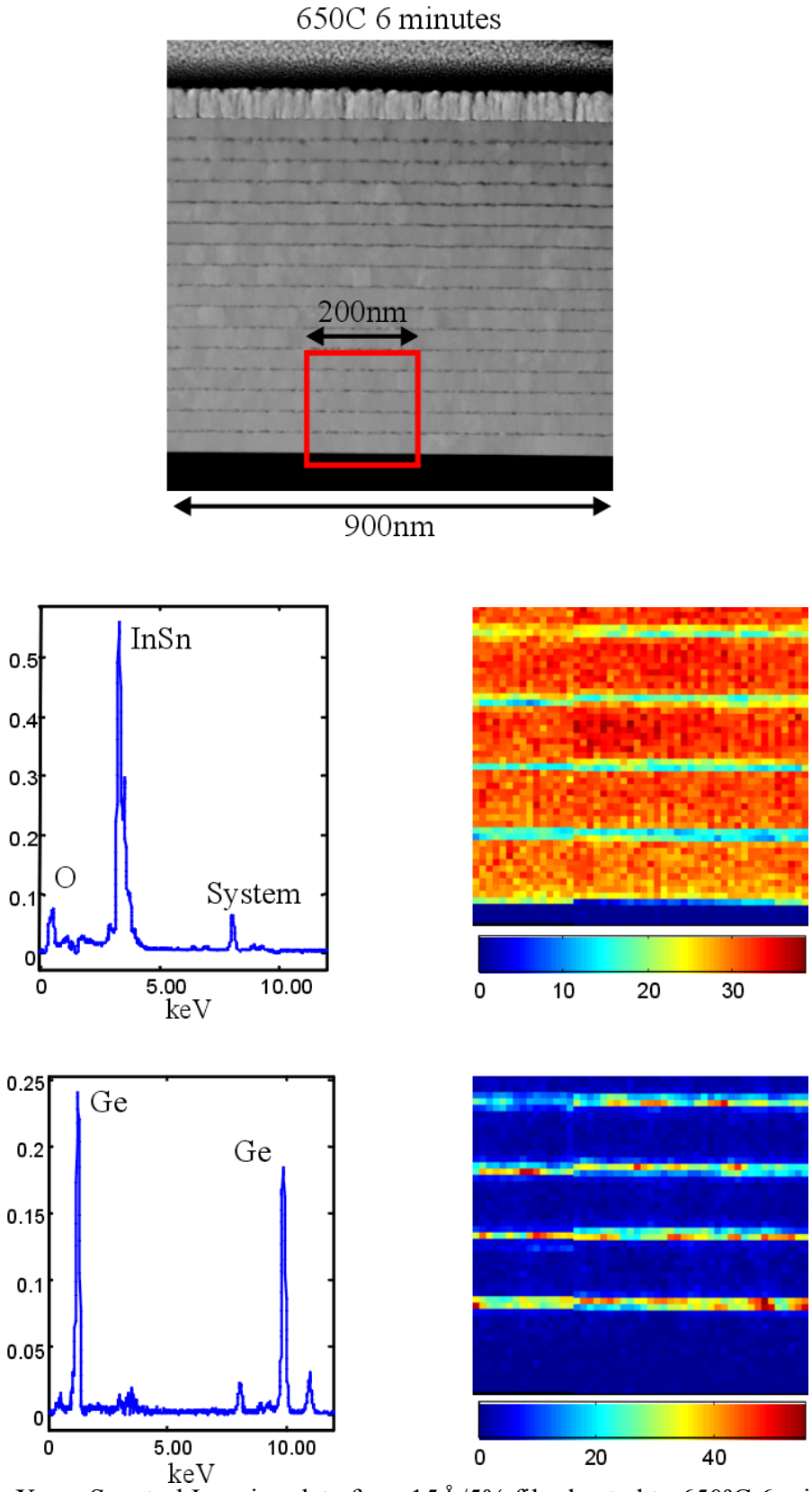

Figure 11 X-ray Spectral Imaging data for a 15Å/5% film heated to 650ºC 6 minutes.

The x-ray automated spectral imaging data helps explain some of the growth processes taking place. At 400ºC the multilayer structure is completely intact, with strong ITO and Ge signals consistent with the image. There is no evidence of any quantum dot formation or any materials interactions taking place. When heated to 600ºC for one hour the film shows definite signs of Ge diffusion both within the Ge layer as well as some diffusion between adjacent Ge layers. These diffusion processes lead to the formation of small dot-like structures within the Ge layers. Again, the chemical signatures detected indicate ITO and Ge where they would be expected. Note, however, that the Ge signature is showing increased signals of O and In/Sn. This could mean that there is some reaction occurring between the Ge and the ITO. But it could also be due to the fact that the x-ray data from the TEM sample is taken over a thickness. This means that it could be detecting some of the ITO matrix material that is present behind the Ge layer. This could be the case when the Ge dots become isolated or if the cross-sectional sample is not exactly normal to the plane of the detector. When a film is annealed to 650ºC for 6 minutes, such a short time allows some inter-diffusion of the Ge, but prohibits the intralayer-diffusion between the Ge layers. What results are dot-like structures of Ge beginning to separate out from the once continuous Ge layers. The chemical signature is strongly Ge, with little to no contributions indicated from the ITO. Again, if any materials interactions are to take place, such short time anneals seem to have prevented it. This may not be the case in the film heated to 660ºC for 30 minutes. This film shows pronounced dot formation within the Ge layers with an average size of 16 nm, but seemingly larger at the bottom of the film. The SI data indicates intralayer and interlayer diffusion of Ge and suggests that the Ge diffuses along the ITO grain boundaries. There is also an increased presence of In/Sn and O in the Ge chemical signature. This combined with the knowledge that much diffusion is present, leads one to think that there is a reaction occurring between the ITO and the Ge. However, the Ge signature is still predominantly Ge, indicating that it may just be surface reactions. Finally, at 700ºC for 12 minutes, the film contains many isolated Ge quantum dots surrounded by ITO. This is supported by the corresponding SI data. All of the SI data as a function of temperature concludes that, in fact, Ge quantum dots are able to form within the ITO up to 700ºC. This is further substantiated by the supporting Raman data of the annealed multilayer films.

For films heated at 700ºC for longer times or above 700ºC, the microstructure and chemical make-up of the films begins to change. It is beyond 700ºC that we leave the workable processing range for quantum dot formation in this materials system. Figures 4-23 – 4-26 illustrate the process of pore formation within the films. It seems that, indeed, there is a materials interaction occurring between the Ge and the ITO, which is facilitated at high temperatures. The first step in the growth process is the desired growth of Ge quantum dot structures. However, over time and at elevated temperatures, the Ge quantum dots begin to diffuse and ripen, creating large particles of Ge. It is during this process that the Ge and the ITO can react. The formation of bubble structures on the surface implies the presence of a volatile species. X-ray data are not conclusive, but suggest that it is an $In_2Ge_2O_7$ phase. At high enough temperatures, something interesting happens that reduces the Ge content in the films and leaves behind pore structures. It was reported by Sarkisov et al. in 1971 that the $In_2Ge_2O_7$, upon an increase in temperature,

decomposes and a gaseous phase of O_2 and GeO evolves [38]. The presence of a gaseous material escaping the composite multilayer films was observed by STEM microscopy where bubble formations were evident in the films heated at and above 700ºC. This posed an upper limit on the workable processing range for Ge quantum dot formation in this materials system.

Optical Properties

Absorbance Data

Figure 1 shows the quantum confinement effect in Ge nanocrystals when isolated in an insulating silica matrix. However, because the matrix material in this study is ITO instead of silica, the degree to which the band edges are shifted is not known. In order to understand and interpret any shifts present in the data, the band edges for the pure ITO and Ge materials must first be established. It is of interest to see images of the actual ITO samples in both the as-deposited state and in the annealed state. Figure 12(a) and (b) shows how the ITO appears both before heat treatment (a) and after being annealed to 1000ºC for 1 hour (b). Figure 13 illustrates this effect in the absorbance edges in ITO films. From the as-deposited state to an anneal temperature of 600ºC, the measured band gap of these ITO films ranges from 4.45 eV to 5.18 eV. It is seen from the absorption plot in Figure 14, that the as-deposited ITO film has the lowest band gap, while the film annealed to 400ºC has the highest measured band gap. It is clear that for temperatures up to 600ºC an increase in E_g is seen.

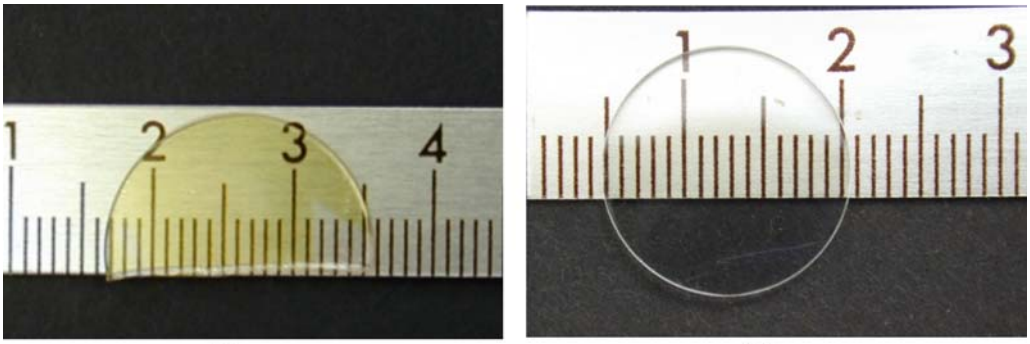

(a) (b)

Figure 12 Photographic images of pure indium tin oxide films (a) in the as-deposited state and (b) annealed to 1000°C for 1 hour.

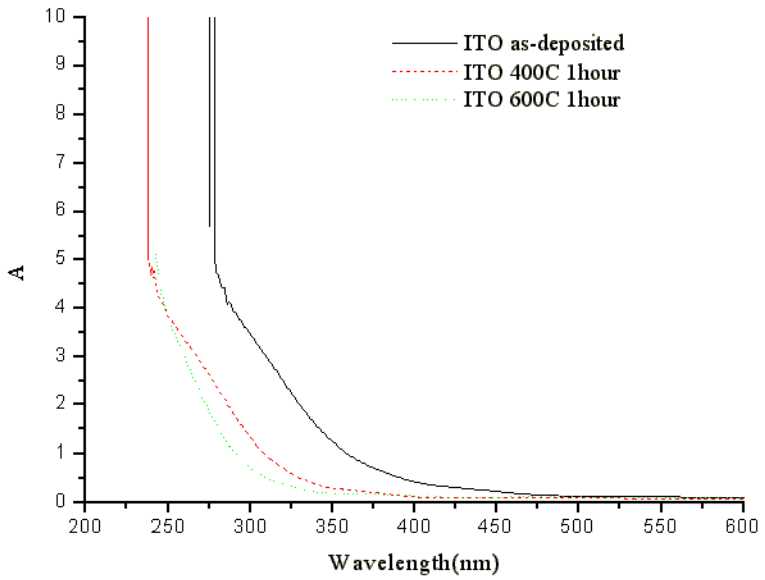

Figure 13 Absorbance data for indium tin oxide films in the as-deposited state, annealed to 400°C for 1 hour, and annealed to 600°C for 1 hour.

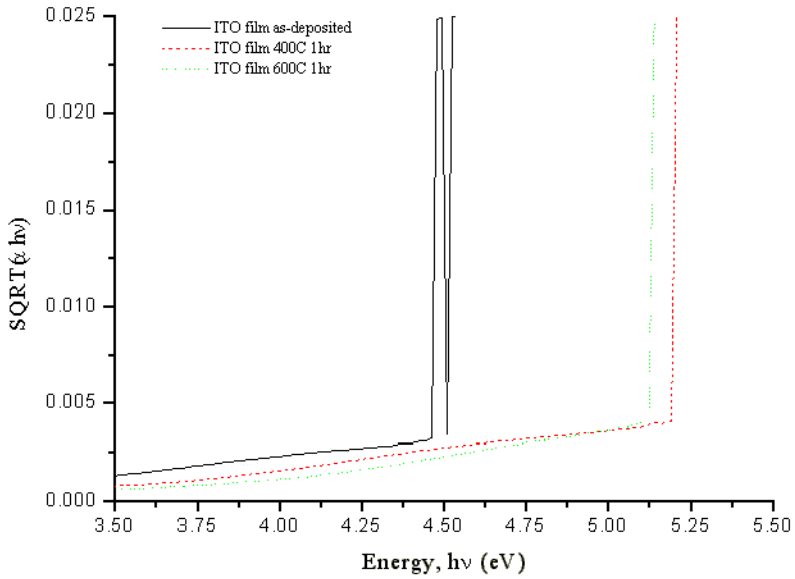

Figure 14 Plot of sqrt(α hν) versus energy, hν, for indium tin oxide films in the as-deposited state, annealed to 400°C 1hour, and annealed 600°C 1 hour.

Figure 15 shows absorbance data for several composite films heat-treated at various times and temperatures. The absorbance data for the ITO film heated to 600ºC for one hour is provided as a reference point. What is obvious is the shifting of the edges that occurs in the quantum dot films. A clear blue-shift in energy takes place due to the presence of the Ge quantum dot structures within the ITO film up to anneal temperatures of 660ºC. However, at 700ºC, the absorbance edge red-shifts, likely due to an overall growth of the Ge dots.

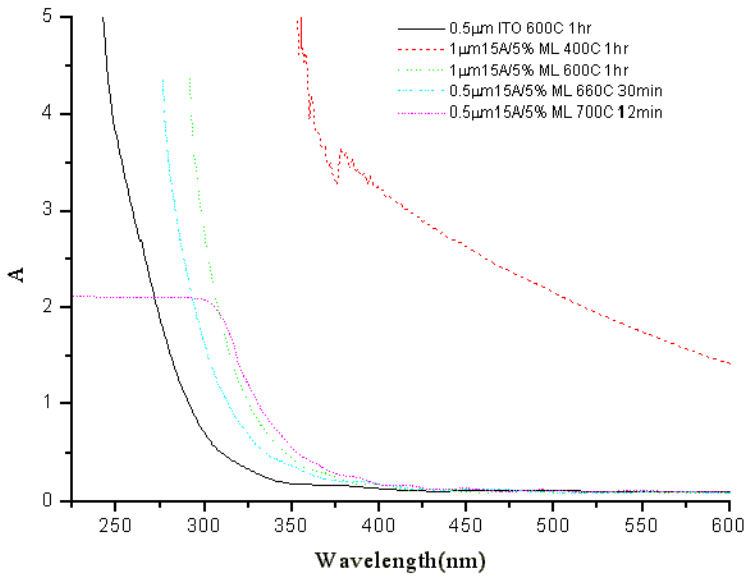

Figure 15 A data for 15Å/5% composite multilayer films at various temperatures.

For the temperature range from the as-deposited state to 600ºC, E_g in the pure ITO films shifts from 4.46 eV to 5.18 eV, respectively. This provides the low-wavelength end limit for the multilayer films. It should be noted that all of the measured band edges for the rf sputtered ITO films are in the range of the published data for ITO. Also, they exhibit very good transparency, especially in the visible wavelength range.

Similarly, the pure Ge film band edge provides the long wavelength end limit. The pure Ge film shows an indirect bandgap with energy near 0.8 eV. This compares reasonably well with published data for partially amorphous Ge thin films [39].

In going from a 15Å/5% Ge mulitlayer film annealed to 400ºC to a similar film annealed to 600ºC, a blue-shift occurs from 3.52 eV to 4.27 eV. Upon further increase in the anneal temperature, the STEM images show that isolated quantum dots appear in the 660ºC 30 minute composite film. This is reflected in the absorbance data as the edge is shifted even farther toward shorter wavelengths, with a corresponding E_g of 4.5 eV. However, for the film heated to 700ºC for 12 minutes, the absorbance edge is red-shifted relative to the 660ºC film to an E_g of 3.91 eV. This implies that the quantum confinement effect is not as strong because of a growth in the size of the quantum dots. This seems to

agree with the computed ranges of the quantum dot sizes reported previously. Also, this agrees with what would be expected intuitively. An increase in temperature allows the diffusion of the germanium to occur more quickly, providing the conditions for Oswald ripening of the dots. This ripening of the Ge was apparent from the spectral imaging data. It should be noted that stress effects can also produce a shift in the band gap energy of a material. However, stress can not account for the dramatic band gap shifts observed in these films.

Photoconductivity

In order to test for a change in conductivity due to photoinduced processes, the four-point probe head was mounted onto an optics table with the appropriate light source directed to the area being probed. With light incident on the film, the resulting voltage drop measured between the probe tips at constant current is monitored as a function of time, before illumination, during illumination and after the light source is removed. In this way, a measure of the response of the film can be established and compared with other films. In this case, the voltage drop measured is the voltage developed between the inner probe tips for a constant current running between the outer probes. Hence, a drop in the voltage measured under illumination conditions is indicative of an increase in the conductivity of the film. The current source and voltage measurement device was a Keithley 236 Source-Measure Unit, which had the capability of simultaneously sourcing the current and measuring for low voltage samples with a sensitivity of 10 μV. Note that for the measurements taken there was a very small noise component of ±0.1 mV.

To prove that any change in conductivity measured is a result of the photoexcitation of carriers from the germanium quantum dots two different wavelengths of light were used. It is important that the first wavelength corresponds to an area in the absorption spectrum where little or no absorption is present. In this way, a baseline measurement can be made where no change in conductivity is expected for either the ITO or multilayer films. For this, an 800 nm Ti:sapphire ring laser was used at a power of 100-300 mW. Then, a wavelength source was chosen within the band edges of the films to ensure that absorption was taking place to produce the necessary excess carriers needed to create an enhanced photoresponse. For this an Ar+ laser fitted with UV optics and tuned to 300 nm was used at a power of 100 mW. It is important to note that the four-point probe measurements were very sensitive to the amount of pressure applied to the film. The measurements could vary for the same film depending on the imparted pressure. To avoid a pressure dependence in the photoconductivity data, all tests performed were done using consistent, constant pressure. Although the readings were pressure dependent, the relative changes in the photoresponses were reproducible for each film tested.

Figure 16 is a plot of the optical absorbance spectra for the films studied in the photoconductivity measurements. The point to notice is where the band edges lie relative to the two light wavelengths used. The films being compared include two ITO films annealed to 600ºC and 800ºC for one hour, and 15Å/5% multilayer films that each have

been annealed to 650ºC for 6 minutes, 660ºC for 30 minutes, and 700ºC for 30 minutes. In all of the films no strong absorption effects are observed at the 800 nm wavelength, while the 300 nm wavelength is within the absorption band edges of all the films tested.

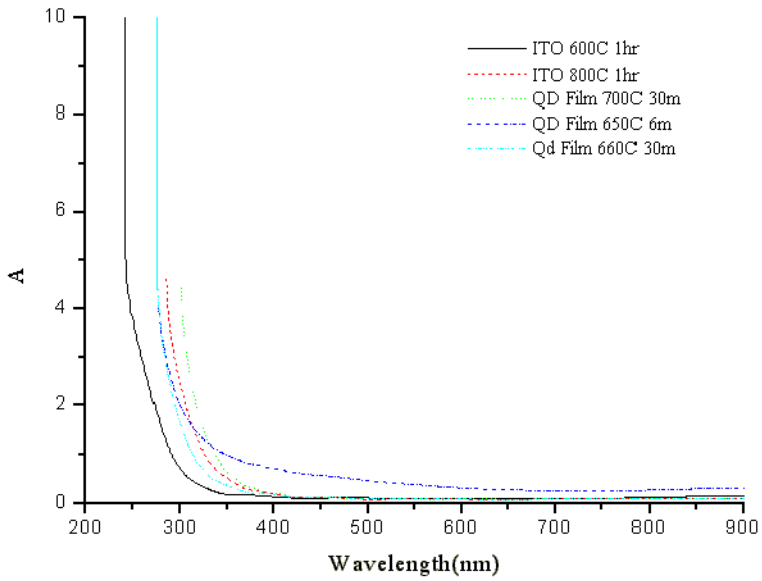

Figure 16 Absorbance data for various ITO and Ge/ITO multilayer films.

Table 5 presents the photoconductivity data measured for the films at 800 nm. Listed are the voltage readings both before, V_b, and after, V_a, illumination, the corresponding change in resistivity and the percent change in conductivity, $\Delta\sigma$, due to the incident light. As expected, there is almost no change ±0.1mV in the electronic response to the 800 nm wavelength light in both the ITO films and the multilayer films.

Table 5 Photoconductivity data for films taken at 800 nm.

Film	Film thickness (μm)	Applied current (mA)	V_b (V)	V_a (V)	$\Delta\rho$ (Ω-cm)	σ_b $(\Omega\text{-cm})^{-1}$	$\%\Delta\sigma$
ITO 600°C	0.5	10	.3141	.3138	6.75E-6	148.0	.10±0.03
ITO 800°C	0.5	5	.2750	.2748	9.00E-6	84.6	.07±0.04
ML 650°C	0.5	1	.1087	.1084	6.45E-5	42.8	.28±0.09
ML 660°C	0.5	1	.2415	.2411	8.60E-5	19.3	.16±0.04
ML 700°C	1.0	10	.4084	.4081	1.29E-5	56.9	.07±0.02

Figure17 is the conductivity data as a function of time for a 15Å/5% multilayer film annealed to 650ºC for 6 minutes. Clearly, there is an enhanced response to the incident light from the film containing the germanium quantum dots. Table 6 summarizes the maximum changes in conductivity under exposure for each film presented. Included are the voltage readings both before, V_b, and after, V_a, light exposure, the measured conductivity before exposure, σ_b, and the resulting percent

increase in conductivity, %Δσ, due to exposure. To illustrate the point that the photoresponse of the multilayer films are much enhanced over the ITO films, Figure 18 presents a normalized plot of the voltage change for the ITO film heated to 600ºC and the multilayer film heated to 660ºC.

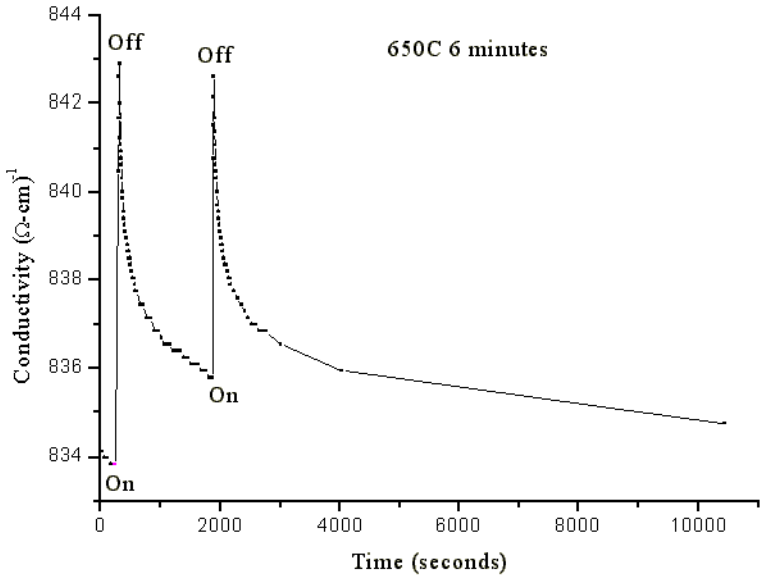

Figure 17 Conductivity versus time for the photoresponse of an 15Å/5% multilayer film heated to 650°C for 6 minutes.

Table 6 Photoconductivity data for films taken at 300 nm.

Film	Film thickness (μm)	Applied current (mA)	V_b (V)	V_a (V)	σ_b $(\Omega\text{-cm})^{-1}$	%Δσ
ITO 600°C	0.5	100	.1479	.1481	3144.7	-0.1±.06
ITO 800°C	0.5	100	.2667	.2662	1744.0	0.2±.04
ML 650°C	0.5	100	.5578	.5518	834.8	1.1±.02
ML 660°C	0.5	10	.2150	.2067	216.4	3.9±.05
ML 700°C	1.0	100	.4170	.4135	557.7	0.8±.02

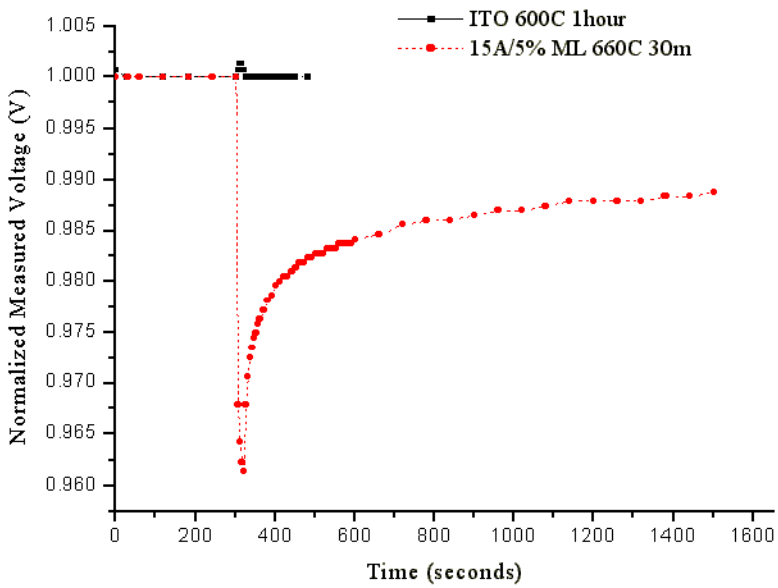

Figure 18 A normalized plot of the measured voltage response versus time for an ITO film heated to 600°C and a multilayer film heated to 660°C.

As seen in Fig. 16 there is little absorption taking place at 800 nm in all of the films compared. This fact is mirrored in the photoresponse of both the ITO films and the multilayer films. In both there was little or no change in the measured voltage under exposure to the light. Remember that the expectation is that for the films containing the germanium quantum dots, any excited carriers created within the dots will be given to the ITO matrix to enhance the electrical response. Clearly at 800 nm the carriers within the germanium will not be excited since it is far below the absorption band edge for these structures. At 300 nm light the situation is very different as there should be sufficient energy to excite carriers within the germanium. For the films containing just indium tin oxide, there is some photoconductive response, but the response is minimal, causing a small increase in conductivity of 0.2% for the 800°C ITO film, and a decrease in the conductivity by 0.1% for the 600°C ITO film. However, the presence of the germanium within the ITO has an enhanced effect on the photoresponse of the multilayer films. Upon exposure to the UV light source the films exhibit an increased electrical response. It is important to note that this effect is reproducible for each film.

Figure 17 presents the conductivity versus time response for the multilayer film heated to 650°C for 6 minutes. Recall from the previous STEM images and XRD data for this film that it consists of small semi-crystalline germanium quantum dots within the continuous germanium layers. Also of importance is the fact that no porosity is present, which has a positive effect on the resulting conductivity. The measured conductivity of the film at time = 0 is 834.14 $(\Omega\text{-cm})^{-1}$. After 20 seconds of illumination to the 300 nm light the conductivity increased to 842.91 $(\Omega\text{-cm})^{-1}$, resulting in an increased conductivity change of $\Delta\sigma = 8.77$ $(\Omega\text{-cm})^{-1}$, corresponding to a 1.1% increase. While fundamentally

this is still a small change, it is an unmistakable increase over the response from the ITO films.

This increased response was also seen in the 660°C multilayer film. It had a base conductivity at time = 0 of 216.33 $(\Omega\text{-cm})^{-1}$, which increased to 225.02 $(\Omega\text{-cm})^{-1}$ after exposure to light, increasing the conductivity by $\Delta\sigma = 8.69$ $(\Omega\text{-cm})^{-1}$, corresponding to a 3.9% increase. This is a further increase in the response seen in the 650°C film discussed above.

CONCLUSIONS

Low-dimensional structures, specifically quantum dots, have proved to be interesting candidate materials for many device applications, including quantum memory and lasers. The purpose of the current study was to investigate the potential of quantum dot thin film structures for use in photoconductive and photovoltaic applications, specifically to show that simultaneous quantum confinement and carrier transfer is possible. In order for this to be established, it must be seen that the presence of quantum dots within the film leads to an enhanced photoresponse over similar films lacking quantum dots. In this study rf magnetron sputtering was used to fabricate multilayered films consisting of germanium, Ge, and indium tin oxide, ITO. The films studied were made up of alternating layers of the materials with an overall content of 5% germanium. Each alternating layer of Ge had a thickness of 15 Å, and each ITO layer had a thickness of 280 Å. Under post-deposition anneals in the temperature range of 600-1000ºC, the continuous germanium layers are transformed into isolated quantum dots surrounded by the transparent, conducting ITO matrix. It is postulated that the germanium quantum dots, when exposed to light of a suitable wavelength, will create excess carriers. In the presence of an applied electric field, the extra carriers would be transported through the conducting matrix to the appropriate contact, producing an enhanced electrical response.

By correlating the microstructural, optical and electrical data from the films, an understanding of the behavior of the germanium quantum, dot multilayer films can be obtained. It was found that, in fact, germanium quantum dots did form within the multilayer structures for anneal temperatures in the range of 600-700ºC for times of 6 minutes to 1 hour. Through micrographs taken with scanning transmission electron microscopy (STEM) and the corresponding x-ray automated spectral imaging data, it was found that small germanium dots 9 nm in size nucleated from the continuous layer around 600ºC. An increase in temperature and time caused the germanium to diffuse within the layer and between layers along the ITO grain boundaries to form larger, isolated dots. Within the temperature range of 600-700ºC, the achievable range of dot sizes was 9 – 25 nm. However, the germanium–indium tin oxide materials system proved reactive at temperatures of 700-1000ºC. In this processing range it was clear that the germanium began to form large particles that ultimately reacted with the surrounding ITO matrix. Although the x-ray data was inconclusive, it seems likely that the reaction forms $In_2Ge_2O_7$ (IGO). IGO is volatile at temperatures near 700ºC, forming a gaseous phase of O_2 and GeO through a decomposition process of $In_2Ge_2O_7 \rightarrow In_2O_3 + O_2 + 2GeO$, consequently leaving behind large pore structures.

To further corroborate the presence of germanium quantum dots within the ITO, Raman and x-ray diffraction, XRD, studies were done. For ITO films there was no obvious Raman peak. The only peaks present in the pure ITO films tested were

contributed by the sapphire substrate. Pure germanium films were grown to examine the corresponding Raman peak, which is centered around 280 and 300 cm-1 for the amorphous and crystalline components, respectively. The theoretical prediction for a shift in the Raman line due to quantum confinement effects states that the center of the peak moves toward smaller wavenumbers. However, it was observed that for the multilayer films, were the Ge Raman peak was present, that the line shifted in the opposite direction. Stress effects can cause such a shifting in the Raman peak, and it was concluded that this was the likely cause behind the observed shift in the films, which overshadowed any effects due to confinement of the germanium. Another trend seen in Raman data due to quantum confinement effects is the softening and broadening of the Raman line with increasing confinement. This effect was observed in the Ge/ITO multilayer films. Similar softening and broadening effects due to quantum confinement also manifest themselves in x-ray diffraction data. This was seen in the multilayer films, where the germanium peak corresponding to (111) plane in a cubic germanium crystal, were broader and less intense in the films containing germanium quantum dots. However, it must be considered that the low intensity of the peaks could be due to the small volume fraction of germanium in the films.

While the STEM micrographs, Raman and XRD data help to support the idea that quantum confinement is playing a role in these multilayer films, the strongest and most obvious evidence comes from the shifting of the band edges observable in UV-Vis absorbance data. When a material is confined to a small dimension, approaching the material's exciton Bohr diameter, then interesting changes occur in the electronic transitions. As the degree of confinement increases, i.e. as the diameter of the material becomes smaller, the band edge is forced to higher energies. This phenomenon was established for the multilayer films containing germanium quantum dots. The absorbance data for films annealed 600-700°C shows a dramatic blue-shift in band gap energy with decreasing dot size, and a corresponding red-shift in energy when the dots grew in size. The shift in the measured absorption edge was consistent with the acquired dot sizes for the films. The most pronounced shift occurred in the film annealed to 660°C for 30 minutes, where isolated germanium quantum dots grew to an average size of 16 nm in diameter. Here, the band gap corresponded to 3.27 eV; an energy significantly higher than the bulk germanium band gap of 0.67 eV. Such a dramatic shifting in the absorption edge, coupled with the data collected from STEM, Raman and XRD, leave little doubt that quantum confinement effects, due to the incorporation of germanium quantum dots, are present in these films.

With germanium dots successfully fabricated into the indium tin oxide matrix the corresponding electrical photoresponse of the films was measured. From a device perspective, by varying the size of the quantum dots many different wavelengths of light can be absorbed and converted into electron–hole pairs. This allows high conversion efficiency of the solar radiation necessary for solar cell technology. The premise for the current research was to prove that a quantum confined material surrounded by a transparent conducting oxide matrix will, under exposure to light with an energy above its band gap, create these excess carriers and, in the presence of an electric field, transport them to the matrix. This would result in an increased electrical response. To prove that the ITO films containing the Ge dots were, in fact, behaving in this fashion, their photoconductive behavior was compared to pure ITO films. It was seen that at 800 nm, a

wavelength below the band gaps of all the films, no significant response in the measured conductivity was present for either the pure or quantum dot films. However, when the response was measured at a wavelength above the band edges of the films, 300 nm, an unmistakable enhancement in the photoresponse was observed for the films containing the germanium dots. Pure ITO films tested showed a response very similar to their response in the below-band gap test, producing an increase in the conductivity under illumination of roughly 0.1%. However, in the quantum dot containing films the enhanced photoconductive response was as high as 3.9%.

While the increases seen in the quantum dot films seem small, it is still a clear indication of the potential that such composite materials can have for creating novel photoconductive and photovoltaic devices. The photoconductive decay curves measured for these films indicate that significant deep level traps are present. By better understanding the nature of these trapping centers and by optimizing the fabrication technique to limit the materials interactions, composite quantum structures such as these could help advance the current state of solar cell technology. The most important contribution of this work is that it experimentally demonstrates that quantum dot structures can simultaneously exhibit a shift in band gap energy resulting from quantum confinement and an increase in photoconductivity resulting from the injection into the conductive matrix of photoexcited carriers created in the quantum dot. This combination of effects promises a better means of harnessing solar energy for use in devices of the future.

LIST OF REFERENCES

1. Tracie J. Bukowski, T.M. Neidt, Romulo Ochoa and Joseph H. Simmons, Journal of Non-Crystalline Solids 274 (2000) p. 87.

2. Joseph H. Simmons, "Novel Design for the Fabrication of High Efficiency Solar Cells," US Patent 5,720,827 February 24, 1998.

3. J.Mort and D. M. Pai, Photoconductivity and Related Phenomena (Elsevier Scientific Publishing Co., New York 1976).

4. Richard H. Bube, Photoconductivity of Solids (John Wiley & Sons, Inc., New York 1971).

5. Roy G. Gordon, MRS Bulletin 25(8) (2000) p. 52.

6. David S. Ginley and Clark Bright, MRS Bulletin 25(8) (2000) p. 15.

7. K.C. Chopra, S. Major and D.K. Pandya, Thin Solid Films 102 (1983) p. 1.

8. S. Nishikawa, Thin Solid Films 135 (1986) p. 219.

9. D.V. Morgan, Thin Solid Films 135 (1995) p. 283.

10. H. Köstlin, R. Jost and W. Lems, Physical State of Solids (a) 29 (1975) p. 87.

11. Martin A. Green, MRS Bulletin 17, No.10 (1993) p. 26.

12. D.V. Morgan, Thin Solid Films 312 (1998) p. 268.

13. K. B. Sundaram and Jila Blanchard, Engineering the New Century Conference Proceedings - IEEE SOUTHEASTCON (1997) p. 230.

14. H. Morikawa and M. Fujita, Thin Solid Films 359 (2000) p. 61.

15. F. Zhu, C.H. A. Huan, Keran Zhang and A.T.S. Wee, Thin Solid Films 359 (2000) p. 244.

16. Wen-Fa Wu and Bi-Shiou Chiou, Thin Solid Films 298 (1997) p. 221.

17. M. Bender, W. Seelig, C. Daube, H. Frankenberger, B. Ocker and J. Stollenwerk, Thin Solid Films 326 (1998) p. 72.

18. E. Terzini, G. Nobile, S. Loreti, C. Minarini, T. Polichetti and P. Thilakan, Japenese Journal of Applied Physics 38 (1999) p. 3448.

19. Wen-Fa Wu, Bi-Shiou Chiou and Shu-Ta Hsieh, Semiconductor Science and Technology 9 (1994) p. 1242.

20. Li-Jian Meng and M. P. dos Santos, Journal of Vacuum Science Technology A 18(4) (2000) p. 1668.

21. E. Terzini, G. Nobile, T. Polichetti and P. Thilakan, IEEE 26th PVSC Conference (1997) p. 667.

22. Yuzo Shigesato, Itaru Yasui and David C. Paine, Journal of Materials March (1995) p. 47.

23. Mamoru Mizuhashi, Thin Solid Films 76 (1981) p. 97.

24. Yutaka Ohhata, Fujitoshi Shinoki and Sadafumi Yoshida, Thin Solid Films 59 (1979) p. 255.

25. F.T.J. Smith and S.L. Lyu, Journal of the Electrochemical Society: Solid-State Science and Technology (1981) p. 2388.

26. Soumyendu Guha, Mark Will and Lloyd Chase, Nuclear Instruments and Methods in Physics Research B 147 (1999) p. 367.

27. Minoru Fujii, Shinji Hayashi and Keiichi Yamamoto, Japanese Journal of Applied Physics 30, No.4 (1991) p. 687.

28. James R. Heath, J.J. Shiang and A.P. Alivisatos, Journal of Chemical Physics 101(2) (1994) p. 1607.

29. M. Zacharias, J. Blasing, M. Lohmann and J. Christen, Thin Solid Films 278 (1996) p. 32.

30. David R. Lide, ed., CRC Handbook of Chemistry and Physics (Academic Press, Inc., Boca Raton 1999).

31. W. E. Beadle ed., Quick Reference Manual For Silicon Integrated Circuit Technology (John Wiley & Sons, Inc., New York 1974).

32. Edward D. Palik, ed., CRC Handbook of Optical Constants of Solids (Academic Press, Inc., Orlando 1985).

33. Melles Griot Company, optical products and support
April 22, 2002. Available.
< www.mellesgriot.com>

34. M. Zacharias, R. Weigand, B. Dietrich, F. Stolze, J. Blasing, P. Veit, T. Drusedau and J. Christen, Journal of Applied Physics 81(5) (1997) p. 2384.

35. B.G. Potter, Dissertation entitled Electronic Band Structure and Optical Characteristics of Quantum-Size CdTe Crystals in Glass Films, University of Florida (1991).

36. John F. O'Hanlon, A User's Guide to Vacuum Technology (John Wiley & Sons, Inc., New York 1989).

37. B.G. Potter and J. H. Simmons, Journal of Applied Physics 68(3) (1990) p. 1218.

38. Sarkisov, Neorg. Mater. 7(2) (1971) p. 341.

39. J. Tauc, R. Grigorovici and A. Vancu, Phys. Status Solidi 15 (1966) p. 627.